

EFFECTS OF VACCINATION ON THE TRANSMISSION DYNAMICS OF COVID-19 IN DOUGHERTY COUNTY OF GEORGIA, USA

BUDDHI PANTHA*

Department of Science and Mathematics Abraham Baldwin Agricultural College Tifton, GA 31793, USA bpantha@abac.edu

JEMAL MOHAMMED-AWEL

Department of Mathematics Morgan State University, Baltimore Maryland 21252, USA jemal.mohammed-awel@morgan.edu

NAVEEN K. VAIDYA

Department of Mathematics San Diego State University San Diego, California 92182, USA

Computational Science Research Center San Diego State University San Diego, California 92182, USA

Viral Information Institute, San Diego State University San Diego, California 92182, USA nvaidya@sdsu.edu

> Received 13 December 2021 Accepted 21 June 2022 Published 13 August 2022

Despite the significant progress in the development of vaccines, the COVID-19 pandemic still poses difficulty for its control because of many obstacles such as the proper implementation of vaccination, public hesitancy towards vaccines, dropping out from the second dose, and varying level of protection after the first and the second doses. In this study, we develop a novel mathematical model of COVID-19 transmission, including two separate vaccinated compartments (first dose and both doses). We parametrize and validate our model using data from Dougherty county of Georgia, USA, one of the most affected counties, where the transmission trend clearly is associated with various policies and public events. We analyze our model for stability of equilibria and persistence of the disease, and formulate expression for reproduction numbers. We estimate that the basic reproduction number in Dougherty county is 1.69, and the effective reproduction number during the study period ranges from 0.26 to 6.36. The number of daily undiagnosed cases peaked at 310 per day, resulting in the maximum number of

^{*}Corresponding author.

active infectious individuals to be 2471. Our model predicts that in a high transmission scenario, the vaccination strategies should be combined with other non-pharmaceutical prevention strategies to ensure transmission control. Moreover, our results emphasize that completing both doses of vaccines on time is critical to achieve maximum benefits from the vaccination programs.

Keywords: COVID-19; Mathematical Model; Undiagnosed; Vaccination; Intervention; Dougherty County of Georgia, USA.

1. Introduction

Coronavirus Disease (COVID-19), caused by SARS-CoV-2, is an ongoing pandemic that has terrified the world with a record number of infections and deaths, disrupting the social, economic, and political conditions of many communities.^{1–3} The disease can spread through the air from infected to susceptible individuals who are physically in close proximity.¹ As of 22 October 2021, more than 243.6 million cases and nearly 5 million deaths worldwide have been reported.^{2,3} The United States has the highest number of COVID-19 cases by far with about 46.2 million cases and more than 754 thousand deaths, the highest numbers in the world, as of 22 October 2021.^{1,2} Several vaccines against the COVID-19 have been developed recently, but the efficacy of these vaccines depends on the vaccine type, circulating virus strain and completion of vaccine doses if more than one dose is required.^{4,5} The emergence of various virus strains, availability of the vaccine, long-term efficacy of the vaccines, public hesitation towards the vaccines, and dropout from the second dose of the vaccine are some of the factors that still pose significant challenges to the control of the disease via vaccination programs.⁵

Georgia is one of the most impacted states of the USA, with about 28,344 deaths and 1.62 million reported cases as of 22 October 2021. Among the 159 counties of Georgia, Dougherty County, a rural county located in the southwest region of the state, had one of the densest clusters of COVID-19 during the early phase of the pandemic (March–April 2020). This county has also suffered from one of the highest per capita deaths in the state during the pandemic.^{6–9} After the first case reported in early March of 2020, the transmission in Dougherty County skyrocketed within a month. State agencies announced some prevention strategies such as shelter-in-place and restriction in business, gathering, and dine-in service. However, weak implementation of these policies, non-masking, public gatherings and protests, may have contributed to the high transmission of the disease. The vaccinations in the county started in mid-February of 2021 with priorities on seniors and immune-compromised people and became available to all public in the last week of March 2021.

Several models have already been developed to study the dynamics of the COVID-19 spread. $^{3,10-20}$ Most of these studies have implemented an extension of the Susceptible–Exposed–Infectious–Recovered (SEIR) type compartmental model and used location-specific recorded positive case data to estimate model parameters. For example, Adhikari *et al.*¹⁷ included immigration of infected individuals in the

SEIR model and considered two compartments of infectious class, recorded positive and non-recorded positive. They studied the effects of non-pharmaceutical intervention strategies, such as lockdown, border screening and quarantine, and detection and isolation, on outbreak indicators such as the number of new cases and the basic reproduction number. Kyrychko et al. 10 developed a compartmental SEIR Model with three different components of the recovered class, asymptomatic recovered, mild symptomatic recovered, and symptomatic/hospitalized recovered. This model also considered populations with age structure and age-specific mixing patterns and the impact of lockdown. Sun and Wang¹² developed an SCIRA compartmental model with susceptible, closely observed or quarantined, infected, recovered, and asymptomatic classes. Their model assumed that the self-recovered from the asymptomatic class become susceptible and also assumed that the recovery depends on the number of hospitalized and quarantined people. Pantha et al. 18 used province-wise data from Nepal to study the effectiveness of universal non-pharmaceutical intervention policies and identified the best policies for each province. They highlighted that the local level study is important for implementing intervention policies.

Some modelers studied the impact of vaccinations together with nonpharmaceutical intervention (NPI) strategies on the disease dynamics. 19-29 For example, Bubar et al.²¹ and Feranna et al.²⁰ used age-structured models to study the impact of vaccines prioritization in different age groups. Their finding shows that vaccine prioritizing the age group of 20–49 years reduces the cumulative incidence, while mortality rate can be reduced by prioritizing adults older than 60. Moreover, they emphasized on vaccinating seronegative individuals to achieve maximum benefits from the vaccination programs. Similarly, Giordano et al.²² highlighted the importance of the vaccines accompanied by non-pharmaceutical interventions to reduce the cases and deaths. Childs et al.^{27–29} developed age-structured SEIR models with vaccination compartment in each age group. They considered waning of vaccine immunity and severity of the disease in their model simulations. They also considered increased transmissibility from novel variants to estimate the impact of relaxing non-pharmaceutical intervention on the disease resurgence. Their results suggest that non-pharmaceutical intervention should be maintained to minimize the chance of resurgence on top of the continued vaccination. It is important to note that the impact of vaccination has been found to depend on the completion of vaccine doses, and there is a significantly different level of protection of vaccines in individuals taking only the first dose and taking both first and second doses of vaccines.³⁰ Therefore, it is critical to distinguish individuals taking only one dose and both doses of vaccines in proper modeling of COVID-19 transmission, and the modeling with the different efficacies of single and double doses of vaccines on the COVID-19 dynamics has not been well explored.

In this study, we developed a mathematical model to study the impact of vaccination on COVID-19 transmission dynamics in Dougherty county, Georgia, USA. While we consider Dougherty county as a case study, our models may also be helpful to guide implementations of vaccination programs in many rural counties

across the nation. The unique feature of our model is its capability to incorporate two compartments of vaccinated individuals (first dose only and both doses) with different levels of protection along with two compartments of infectious individuals (diagnosed and undiagnosed). We validate our model with COVID-19 case data, compiled according to the various events associated with the epidemic trend in Dougherty County. We perform a thorough analysis of the model and formulate the reproduction numbers. Furthermore, we use our model to investigate the effects of various vaccination strategies on the burden of this pandemic in Dougherty County.

2. Mathematical Model

2.1. Model formulation

We formulate a transmission dynamics model consisting of seven compartments: Susceptible (S), Vaccinated with first does (V_1) , Vaccinated with both doses (V_2) , Exposed (E), Undiagnosed Infected (I_u) , Diagnosed Infected (I_d) , and Recovered (R). Two-dose vaccines are usually implemented with a certain time gap between doses, and the protection from the vaccines highly depends on whether only the first dose or both doses are completed.³⁰ Thus, the vaccinated classes with the first

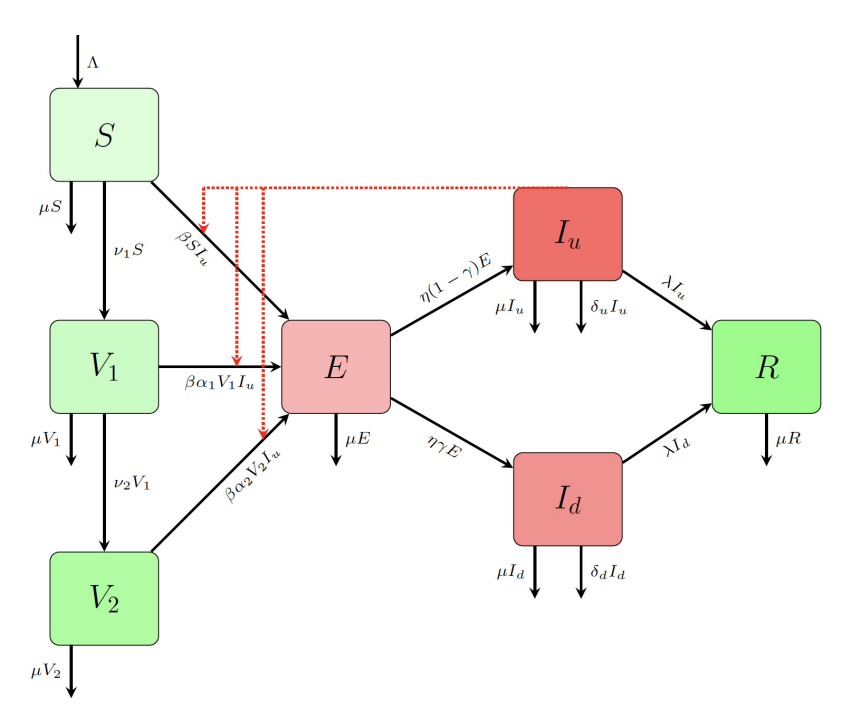


Fig. 1. Schematic diagram of the COVID-19 transmission dynamics with vaccinations. The bold pointed solid lines represent the transfer of individuals to another compartment due to infection or progression. The pointed dotted red lines represent the interaction that causes new infections.

dose (V_1) and with both doses (V_2) have different levels of protection. Figure 1 presents the flow diagram of the population movement between the compartments.

In our model, individuals in all compartments die with a natural death rate μ . The susceptible individuals are recruited with a rate Λ , get vaccinated with a rate ν_1 , and are infected with the COVID-19 virus upon interaction with the undiagnosed infected individuals with a rate β . Individuals in both vaccinated classes can also contract the virus upon contact with the infectious individuals, but with different infection rates. We assume that α_1 and α_2 are the residual susceptibility of the vaccinated individuals in V_1 and V_2 classes, respectively. The individuals vaccinated with the first dose (V_1) receive the second dose with a rate ν_2 . The main difference between the two vaccinated compartments is the different level of protection against the COVID-19 susceptibility: the individuals with two doses of vaccine (complete vaccination) are protected higher than the individuals with one dose of vaccine (incomplete vaccination), i.e., $\alpha_1 > \alpha_2$.

While the vaccinated individuals have been infected and recommended for a booster shot, the actual time and magnitude of the immunity loss have not been quantified. Also, most of the infected individuals who were vaccinated were infected with a different strain. Different protection levels for the different strains can be incorporated into our model through different values of α_1 and α_2 . Because of the uncertainty on the loss of immunity and focus of the study on the single circulating variant, we distinguish two vaccinated groups (one dose and two doses) via their efficacy and ignore the potential waning of vaccine immunity in the short period of our study.

The exposed individuals (E) leave the compartment with rate η among which the fraction γ progress towards diagnosed compartment, (I_d) , and the remaining fraction $1-\gamma$ move toward the undiagnosed compartment, I_u . Since the diagnosed people are mostly in isolation, and also the possibility of infection by hospitalized (infected) individuals is expected to be low due to strict hygiene and protection protocols, we do not consider the potential transmission from diagnosed people. The individuals in diagnosed and undiagnosed infected classes die with rates δ_d and δ_u , respectively, and both recover with a rate λ . The rate of change of people in each compartment can be described by the following system of equations (2.1).

$$\begin{split} \frac{dS}{dt} &= \Lambda - \beta S I_u - \nu_1 S - \mu S, \\ \frac{dV_1}{dt} &= \nu_1 S - \beta \alpha_1 V_1 I_u - \nu_2 V_1 - \mu V_1, \\ \frac{dV_2}{dt} &= \nu_2 V_1 - \beta \alpha_2 V_2 I_u - \mu V_2, \\ \frac{dE}{dt} &= \beta S I_u + \beta \alpha_1 V_1 I_u + \beta \alpha_2 V_2 I_u - \eta E - \mu E, \\ \frac{dI_u}{dt} &= \eta (1 - \gamma) E - \lambda I_u - \delta_u I_u - \mu I_u, \end{split}$$

$$\frac{dI_d}{dt} = \eta \gamma E - \lambda I_d - \delta_d I_d - \mu I_d,$$

$$\frac{dR}{dt} = \lambda I_u + \lambda I_d - \mu R.$$
(2.1)

2.2. Model analysis

2.2.1. Positivity and boundedness of solutions

All the variables in model (2.1) are non-negative and should remain non-negative since they represent human populations. It can be easily verified that model (2.1) has non-negative solutions for non-negative initial conditions. Let $N(t) = S(t) + V_1(t) + V_2(t) + E(t) + I_u(t) + I_d(t) + R(t)$ be the total population.

Theorem 2.1. If N(0) > 0, then the total population, N(t), is bounded below and above by positive numbers, i.e.,

$$0 < N_{\min} \le N(t) \le N_{\max}, \ \forall t,$$

where $N_{\min} = \min\{N(0), \frac{\Lambda}{\mu + \delta_{+} + \delta_{-} l}\}$ and $N_{\max} = \max\{N(0), \frac{\Lambda}{\mu}\}$.

Proof. Since all components are non-negative, adding all equations, we get

$$\frac{dN}{dt} = \Lambda - \mu N - \delta_u I_u - \delta_d I_d. \tag{2.2}$$

Adding μN on both sides, multiplying by the integration factor $e^{\mu t}$, and then integrating the resulting equation from 0 to t, we get

$$N(t) = e^{-\mu t} N(0) + \int_0^t e^{\mu(s-t)} (\Lambda - \delta_u I_u(s) - \delta_d I_d(s)) ds$$

$$\leq e^{-\mu t} N(0) + \int_0^t e^{\mu(s-t)} \Lambda ds = e^{-\mu t} N(0) + \frac{\Lambda}{\mu} (1 - e^{-\mu t}).$$

Note that the derivative of the right-hand side is $\mu e^{-\mu t} (\frac{\Lambda}{\mu} - N(0))$. Thus, it is a monotone function with absolute maximum, $\max\{N(0), \frac{\Lambda}{\mu}\}$. Rewriting Eq. (2.2), we get

$$\frac{dN}{dt} = \Lambda - (\mu + \delta_u + \delta_d)N + \delta_u(N - I_u) + \delta_d(N - I_d).$$

This implies

$$N(t) = e^{-(\mu + \delta_u + \delta_d)t} N(0) + \int_0^t e^{(\mu + \delta_u + \delta_d)(s - t)} (\Lambda + \delta_u (N - I_u) + \delta_d (N - I_d)) ds$$

$$\geq e^{-(\mu + \delta_u + \delta_d)t} N(0) + \frac{\Lambda}{\mu + \delta_u + \delta_d} (1 - e^{-(\mu + \delta_u + \delta_d)t}).$$

Thus, its absolute minimum is $\min\{N(0), \frac{\Lambda}{\mu + \delta_u + \delta_d}\}$.

Also, it can be easily verified that the biologically feasible region $\Omega \subseteq \mathbb{R}^7$ defined by

$$\Omega = \{ (S(t), V_1(t), V_2(t), E(t), I_u(t), I_d(t), R(t)) \in \mathbb{R}_+^7 \mid 0 < (N)_{\min} \le N(t) \le (N)_{\max} \}$$
(2.3)

is positively invariant and attracting for system 2.1, i.e., solutions that initially start from, or enter Ω , remain inside Ω . Therefore, the model system 2.1 is mathematically well-posed. This property of the model is stated in the theorem below.

Theorem 2.2. The biologically feasible region $\Omega \subseteq \mathbb{R}^7_+$ defined by (2.3) is positively invariant and attracting for system (2.1) with given initial conditions in \mathbb{R}^7_+ .

2.2.2. Vaccination reproduction number and disease-free equilibrium

The disease-free equilibrium of system 2.1 is given by

$$E^{0} = (S^{0}, V_{1}^{0}, V_{2}^{0}, E^{0}, I_{u}^{0}, I_{d}^{0}, R^{0})$$

$$= \left(\frac{\Lambda}{\nu_{1} + \mu}, \frac{\nu_{1}\Lambda}{(\nu_{1} + \mu)(\nu_{2} + \mu)}, \frac{\nu_{1}\nu_{2}\Lambda}{\mu(\nu_{1} + \mu)(\nu_{2} + \mu)}, 0, 0, 0, 0\right).$$
(2.4)

In the context of our modeling of COVID-19 transmission under vaccination, the vaccination reproduction number (\mathcal{R}_{vac}) is the average number of secondary infections produced by a typical case of an infection in a population with a proportion $\frac{\mu}{(\nu_1+\mu)}$ is susceptible, a proportion $\frac{\nu_1\mu}{(\nu_1+\mu)(\nu_2+\mu)}$ is vaccinated with the first dose and a proportion $\frac{\nu_1\nu_2}{(\nu_1+\mu)(\nu_2+\mu)}$ is vaccinated with both the first and second doses. Using the next generation matrix approach,³¹ the vaccination reproduction number, \mathcal{R}_{vac} , of model 2.1, is given by the dominant eigenvalue or spectral radius of the next generation matrix \mathcal{FV}^{-1} , where

$$\mathcal{F} = \begin{pmatrix} 0 & \beta \alpha_1 V_1^0 + \beta \alpha_2 V_2^0 + \beta S^0 & 0 \\ 0 & 0 & 0 \\ 0 & 0 & 0 \end{pmatrix} \text{ and }$$

$$\mathcal{V} = \begin{pmatrix} \eta + \mu & 0 & 0 \\ -\eta (1 - \gamma) & \lambda + \delta_u + \mu & 0 \\ -\eta \gamma & 0 & \lambda + \delta_d + \mu \end{pmatrix}.$$

Therefore, the vaccination reproduction number, \mathcal{R}_{vac} , for our model is

$$\mathcal{R}_{\text{vac}} = \frac{\beta \eta (1 - \gamma)(\alpha_1 V_1^0 + \alpha_2 V_2^0 + S^0)}{(\eta + \mu)(\lambda + \mu + \delta_u)}.$$
 (2.5)

Substituting $S^0 = \frac{\Lambda}{\nu_1 + \mu}$, $V_1^0 = \frac{\nu_1 \Lambda}{(\nu_1 + \mu)(\nu_2 + \mu)}$, and $V_2^0 = \frac{\nu_1 \nu_2 \Lambda}{\mu(\nu_1 + \mu)(\nu_2 + \mu)}$ in (2.5), we obtain

$$\mathcal{R}_{\mathrm{vac}} = \frac{\beta \eta (1 - \gamma) \Lambda}{(\eta + \mu)(\nu_1 + \mu)(\lambda + \delta_u + \mu)} \left(\frac{\alpha_1 \nu_1}{\nu_2 + \mu} + \frac{\alpha_2 \nu_1 \nu_2}{\mu(\nu_2 + \mu)} + 1 \right).$$

The following theorem is established from Theorem 2 of Ref. 31.

Theorem 2.3. The disease-free equilibrium, E^0 , of system (2.1) is locally asymptotically stable in Ω when $\mathcal{R}_{vac} < 1$ and unstable when $\mathcal{R}_{vac} > 1$.

2.2.3. Global stability of the disease-free-equilibrium

Define the following regions:

$$\Omega_d = \{ (S(t), V_1(t), V_2(t), E(t), I_u(t), I_d(t), R(t)) \subseteq \Omega \mid 0 \le S(t) \le S^0,$$

$$0 \le V_1(t) \le V_1^0, 0 \le V_2(t) \le V_2^0 \},$$

$$(2.6)$$

Lemma 2.1. The sub-region $\Omega_d \subseteq \Omega$ defined by (2.6) is positively invariant for the model system (2.1).

Proof. For the equation

$$\frac{dS}{dt} = \Lambda - \beta S I_u - \nu_1 S - \mu S,$$

Adding $(\nu_1 + \mu)S$ on both sides, multiplying by the integration factor $e^{(\nu_1 + \mu)t}$, and then integrating the resulting equation from 0 to t, we get

$$S(t) = e^{-(\nu_1 + \mu)t} S(0) + \int_0^t e^{(\nu_1 + \mu)(s-t)} (\Lambda - \beta S I_u(s)) ds$$

$$\leq e^{-(\nu_1 + \mu)t} S(0) + \int_0^t e^{(\nu_1 + \mu)(s-t)} \Lambda ds$$

$$= e^{-(\nu_1 + \mu)t} S(0) + \frac{\Lambda}{\nu_1 + \mu} (1 - e^{-(\nu_1 + \mu)t}).$$

Since the derivative of the right-hand side is $(\nu_1 + \mu)e^{-(\nu_1 + \mu)t}(\frac{\Lambda}{\nu_1 + \mu} - S(0))$, if $S(0) \leq S^0 = \frac{\Lambda}{\nu_1 + \mu}$, then S(t) is an increasing function with absolute maximum $\frac{\Lambda}{\nu_1 + \mu}$. That is $S(t) \leq S^0$ for all $t \geq 0$ if $S(0) \leq S^0$. Similarly, it can be shown that $V_1(t) \leq V_1^0$ and $V_2(t) \leq V_2^0$ for all $t \geq 0$, if $V_1(0) \leq V_1^0$ and $V_2(0) \leq V_2^0$, respectively. Thus, the set Ω_d is positively invariant under the system 2.1.

To show the global stability of E^0 in Ω_d , we first decompose the model system (2.1) into two subsystems

$$\frac{dX}{dt} = F(X, I)$$
 and $\frac{dI}{dt} = G(X, I)$,

where $X = (S, V_1, V_2, R) \in \mathbb{R}^4_+$ and $I = (E, I_u, I_d) \in \mathbb{R}^3_+$ are vectors of uninfected and infected individuals, respectively. The following theorem is established using the technique introduced previously.³²

Theorem 2.4. The disease-free equilibrium, $E^0 = (X^0, 0)$ of the system (2.1) is globally asymptotically stable (g.a.s) in $\Omega_d \subseteq \Omega$, provided that $\mathcal{R}_{vac} < 1$ (locally asymptotically stable) and that the following conditions are satisfied:

- (i) For $\frac{dX}{dt} = F(X,0)$, the equilibrium $X^0 = (S^0, V_1^0, V_2^0, 0)$ is g.a.s, (ii) $G(X,I) = AI \tilde{G}(X,I), \tilde{G}(X,I) \geq 0$ for $(X,I) \in \Omega_d$, where $A = D_I G(X^0, 0)$ is an M-matrix (the off diagonal matrix of A are nonnegative) in Ω_d .

Proof. By Castillo-Chavez et al., 32 it is sufficient to show that conditions (i) and (ii) are satisfied if $\mathcal{R}_{\text{vac}} < 1$. From (2.1), we have

$$F(X,I) = \begin{pmatrix} \Lambda - \beta S I_u - \nu_1 S - \mu S \\ \nu_1 S - \beta \alpha_1 V_1 I_u - \nu_2 V_1 - \mu V_1 \\ \nu_2 V_1 - \beta \alpha_2 V_2 I_u - \mu V_2 \\ \lambda I_u + \lambda I_d - \mu R \end{pmatrix}, \text{ and }$$

$$G(X,I) = \begin{pmatrix} \beta S I_u + \beta \alpha_1 V_1 I_u + \beta \alpha_2 V_2 I_u - \eta E - \mu E \\ \eta (1 - \gamma) E - \lambda I_u - \delta_u I_u - \mu I_u \\ \eta \gamma E - \lambda I_d - \delta_d I_d - \mu I_d \end{pmatrix}.$$

By differentiating G(X,I) with respect to I and substituting (X,0), we obtain

$$A = \begin{pmatrix} -(\eta + \mu) & \beta S^0 + \beta \alpha_1 V_1^0 + \beta \alpha_2 V_2^0 & 0 \\ \eta (1 - \gamma) & -(\lambda + \delta_u + \mu) & 0 \\ \eta \gamma & 0 & -(\lambda + \delta_d + \mu) \end{pmatrix} \quad \text{and}$$

$$\tilde{G}(X,I) = \begin{pmatrix} \beta(S^0 - S(t)) + \beta\alpha_1(V_1^0 - V_1(t)) + \beta\alpha_2(V_2^0 - V_2(t)) \\ 0 \\ 0 \end{pmatrix}.$$

Clearly, A is M-matrix, $\tilde{G}(X,I) \geq 0$ for $(X,I) \in \Omega_d$. Furthermore, $X^0 = (S^0, V_1^0, V_2^0, 0)$ is a g.a.s equilibrium of $\frac{dX}{dt} = F(X,0)$ (if $\mathcal{R}_{\text{vac}} < 1$). Therefore, the conditions (i) and (ii) are satisfied if $\mathcal{R}_{\text{vac}} < 1$. Hence, E^0 is g.a.s by the results in Castillo-Chavez et al. [32].

2.2.4. Existence of unique endemic equilibrium

Let $K_1 = \nu_1 + \mu$, $K_2 = \nu_2 + \mu$, $K_3 = \eta + \mu$, $K_4 = \lambda + \delta_u + \mu$, and $K_5 = \lambda + \delta_d + \mu$. The endemic equilibrium of the system (2.1) is given by

$$E^* = (S^*, V_1^*, V_2^*, E^*, I_u^*, I_d^*, R^*).$$

The endemic equilibrium values of $S^*, V_1^*, V_2^*, E^*, I_u^*, I_d^*$ and R^* are expressible in terms of the equilibrium value of I_u^* as follows:

$$S^* = \frac{\Lambda}{\beta I_u^* + K_1}, \quad V_1^* = \frac{\nu_1 \Lambda}{(\beta I_u^* + K_1)(\beta \alpha_1 I_u^* + K_2)}, \quad E^* = \frac{K_4 I_u^*}{\eta (1 - \gamma)},$$

$$V_2^* = \frac{\nu_1 \nu_2 \Lambda}{(\beta I_u^* + K_1)(\beta \alpha_1 I_u^* + K_2)(\beta \alpha_2 I_u^* + \mu)}, \quad I_d^* = \frac{\gamma K_4 I_u^*}{(1 - \gamma)K_5}, \quad \text{and}$$

$$R^* = \frac{(\lambda (1 - \gamma)K_5 + \lambda \gamma K_4)I_u^*}{(1 - \gamma)\mu K_5}.$$

Here, I_u^* is the solution of the following cubic equation, obtained by substituting the equilibrium values of $S^*, V_1^*, V_2^*, E^*, I_u^*, I_d^*$ and R^* into the right-hand side of the equations from (2.1)

$$I_{u}^{*}(a_{3}(I_{u}^{*})^{3} + a_{2}(I_{u}^{*})^{2} + a_{1}I_{u}^{*} + a_{0}) = 0,$$
(2.7)

where

$$a_{3} = K_{4}K_{4}\alpha_{1}\alpha_{2}\beta^{3},$$

$$a_{2} = \Lambda\alpha_{1}\alpha_{2}\beta^{3}\eta(1-\gamma) + K_{1}K_{3}\alpha_{1}\alpha_{2}\beta^{2}\eta + K_{1}K_{3}\alpha_{1}\alpha_{2}\beta^{2}\mu$$

$$+ K_{2}K_{3}\alpha_{2}\beta^{2}\eta + K_{2}K_{3}\alpha_{2}\beta^{2}\mu + K_{3}\alpha_{1}\beta^{2}\eta\mu + K_{3}\alpha_{1}\beta^{2}\mu^{2},$$

$$a_{1} = \Lambda\alpha_{1}\alpha_{2}\beta^{2}\eta\nu_{1}(1-\gamma) + K_{2}\Lambda\alpha_{2}\beta^{2}\eta(1-\gamma) + \Lambda\alpha_{1}\beta^{2}\eta\mu(1-\gamma)$$

$$+ K_{1}K_{2}K_{4}\alpha_{2}\beta\eta + K_{1}K_{2}K_{4}\alpha_{2}\beta\mu + K_{1}K_{4}\alpha_{1}\beta\eta\mu + K_{1}K_{4}\alpha_{1}\beta\mu^{2}$$

$$+ K_{2}K_{4}\beta\eta\mu + K_{2}K_{4}\beta\mu^{2}, \text{ and}$$

$$a_{0} = K_{1}K_{2}K_{3}K_{4}\mu(1-\mathcal{R}_{\text{vac}}).$$

This implies

$$I_{u}^{*} = 0$$
, or (2.8)

$$a_3(I_u^*)^3 + a_2(I_u^*)^2 + a_1I_u^* + a_0 = 0, (2.9)$$

The solution $I_u^* = 0$ corresponds to the disease-free equilibrium of the system 2.1 discussed in Sec. 2.2.2.

In Eq. (2.9), $a_3 > 0$, $a_2 > 0$ and $a_1 > 0$. Also, $a_0 < 0$ if and only if $\mathcal{R}_{\text{vac}} > 1$. Therefore, the coefficients of Eq. (2.7) and Descartes rule of signs can be applied to conclude that the polynomial equation in (2.7) has exactly one positive root if $\mathcal{R}_{\text{vac}} > 1$ and has no positive root if $\mathcal{R}_{\text{vac}} < 1$. Also, if $\mathcal{R}_{\text{vac}} = 1$, $a_0 = 0$ and Eq. (2.9) becomes $I_u^*(a_3(I_u^*)^2 + a_2(I_u^*) + a_1) = 0$. This equation has a solution $I_u^* = 0$, which corresponds to the disease-free equilibrium, and no positive solution since $a_3(I_u^*)^2 + a_2(I_u^*) + a_1 = 0$ has no positive solution by Descartes rule of signs. Thus, the following result is established.

Theorem 2.5. The system (2.1) has unique positive endemic equilibrium (E^*) if and only if $\mathcal{R}_{vac} > 1$.

In the theorem below, we will show that the infected populations E, I_u , and I_d remain persistent for $\mathcal{R}_{\text{vac}} > 1$.

Theorem 2.6. If $\mathcal{R}_{vac} > 1$, then the disease is uniformly persistent in the sense that there exists an $\varepsilon > 0$ such that for every positive solution of (2.1), the following inequality holds:

$$\liminf_{t\to\infty} E(t) > \varepsilon, \quad \liminf_{t\to\infty} I_u(t) > \varepsilon, \quad \text{and} \quad \liminf_{t\to\infty} I_d(t) > \varepsilon.$$

Proof. A theorem by Thieme³³ is used to prove the uniform persistence of the disease. Let

$$L = (S, V_1, V_2, R, E, I_u, I_d), \quad \tilde{L} = (E, I_u, I_d),$$

$$Q = \{L \in \mathbb{R}^7_+ | L_i \ge 0, i = 1, \dots, 7, \text{ where } L_i \text{ is the } i \text{th component of } L\},$$

$$Q_0 = \{L \in Q | L_i > 0, i = 5, \dots, 7\} \quad \text{and}$$

$$P = Q/Q_0 = \{L \in Q | L_i = 0, \text{ for some } i = 5, \dots, 7\}.$$

We will show that system (2.1) is uniformly persistent with respect to (Q_0, P) . Since P contains a single equilibrium, E^0 , it is sufficient to show that $W^s(E^0) \cap Q_0 = \emptyset$, where the set $W^s(E^0)$ denotes the stable manifold of the disease-free equilibrium, E^0 . Suppose this is not true, then there is a solution $(S, V_1, V_2, R, E, I_u, I_d) \in Q_0$ of (2.1) such that

$$\lim_{t \to \infty} (S(t), V_1(t), V_2(t), R(t), E(t), I_u(t), I_d(t)) = (S^0, V_1^0, V_2^0, 0, 0, 0, 0),$$

where
$$S^0 = \frac{\Lambda}{\nu_1 + \mu}$$
, $V_1^0 = \frac{\nu_1 \Lambda}{(\nu_1 + \mu)(\nu_2 + \mu)}$, and $V_2^0 = \frac{\nu_1 \nu_2 \Lambda}{\mu(\nu_1 + \mu)(\nu_2 + \mu)}$.

Then for any $\xi>0$, we have $S^0-\xi\leq S(t)\leq S^0+\xi,\ V_1^0-\xi\leq V_1(t)\leq V_1^0+\xi,\ V_2^0-\xi\leq V_2(t)\leq V_2^0+\xi,$ and $0\leq L_i(t)\leq \xi,\ i=5\dots 7,$ for large t. It

follows from the system (2.1) that

$$\begin{split} \begin{pmatrix} \dot{E} \\ \dot{I}_u \\ \dot{I}_d \end{pmatrix} &= \begin{pmatrix} \beta S I_u + \beta \alpha_1 V_1 I_u + \beta \alpha_2 V_2 I_u \\ 0 \\ 0 \end{pmatrix} \\ &+ \begin{pmatrix} -(\eta + \mu) & 0 & 0 \\ \eta (1 - \gamma) & -(\lambda + \delta_u + \mu) & 0 \\ \eta \gamma & 0 & -(\lambda + \delta_d + \mu) \end{pmatrix} \begin{pmatrix} E \\ I_u \\ I_d \end{pmatrix} \\ &\geq \begin{pmatrix} -(\eta + \mu) & \beta S^0 + \beta \alpha_1 V_1^0 + \beta \alpha_2 V_2^0 - \tilde{l}(\xi) & 0 \\ \eta (1 - \gamma) & -(\lambda + \delta_u + \mu) & 0 \\ \eta \gamma & 0 & -(\lambda + \delta_d + \mu) \end{pmatrix} \begin{pmatrix} E \\ I_u \\ I_d \end{pmatrix} \\ &= \tilde{J}(\xi) \tilde{L}, \end{split}$$

where $\tilde{l}(\xi) = \xi \beta (1 + \alpha_1 + \alpha_2)$, and

$$\tilde{J}(0) = \begin{pmatrix} -(\eta + \mu) & \beta S^0 + \beta \alpha_1 V_1^0 + \beta \alpha_2 V_2^0 & 0 \\ \eta (1 - \gamma) & -(\lambda + \delta_u + \mu) & 0 \\ \eta \gamma & 0 & -(\lambda + \delta_d + \mu) \end{pmatrix}.$$

Observe that $\tilde{J}(0)$ is equal to $(\mathcal{F} - \mathcal{V})$, and has at least one eigenvalue with positive real part if $\mathcal{R}_{\text{vac}} > 1$. Since $\xi > 0$ is arbitrary, $s(\tilde{J}(\xi))$ is positive for small enough $\xi > 0$, where s(A) is the largest real part of the eigenvalues of a matrix A. Therefore, there exist solutions of the linear system

$$\dot{\tilde{L}} = \tilde{J}(\xi)\tilde{L},$$

that grow exponentially. This is a contradiction since solutions to system (2.1) are ultimately bounded (in Ω). Hence, $W^s(E^0) \cap Q_0 = \emptyset$. Using Theorem 4.6 in Ref. 33, it can be concluded that the system (2.1) is uniformly persistent with respect to (Q_0, P) .

3. Model Validation: Case Data from Dougherty County, GA, USA

3.1. Outbreak data, intervention policies, and public events

We compile the Dougherty county data of daily diagnosed cases for over 14 months from 14 March 2020 to 31 May 2021.³⁴ The first positive case in Dougherty County was reported on 10 March 2020.^{6,7} Just within a few days, the virus was spread in the community, affecting healthcare workers as well. The high burden of the hospitalized patients and limited resources made the situation dire, and the employees, who tested positive without showing symptoms, were also asked to work.³⁵ All

public elementary, secondary, and post-secondary schools in Georgia were ordered to be closed effective from 18 March 2020. The order for school closure was later extended to the entire 2019–2020 school year. Effective from 23 March 2020, the state-imposed restrictions on public gathering and enforced social distancing. Due to the rapid increase in the reported cases, the state implemented shelter-in-place starting from 2 April 2020, for two weeks and is later extended to 30 April 2020. The reported cases in Dougherty County peaked on 23 March–18 April 2020 with daily cases peaked as high as 251 (7 April 2020). This period was considered the worst in the state and contained one of the highest per capita infections in the entire country.⁶⁻⁹

The number of reported cases decreased after implementing restrictions such as shelter-in-place (2 April 2020) and limitations on gatherings (14 June 2020). But the immediate spike in the reported cases was observed after the termination of such restriction policies, such as the end of shelter-in-place on 30 April 2020, for adults and 14 June 2020, for seniors. The spike particularly appeared during increased public events with gatherings and protests during May 2020, November, 2020, December 2020, and January 2021. The phase-wise vaccination in Dougherty county started on 22 February 2021, and was made available to the general public age 16 and older on 25 March 2021. After the initiation of vaccination, the number of new positive cases remained at relatively low levels.

3.2. Parameter estimation

Initial Values. According to the United States Census Bureau, the population estimate for 2019 in Dougherty county is $87,965,^{36,37}$ with a yearly estimated decay rate of 1.42%. This implies that the population estimate for 2020 is S(0) = 86,712. Since there were no vaccines available for the general public before 2021, the initial number of vaccinated people is taken as zero, i.e., $V_1(0) = V_2(0) = 0$. The initial number of diagnosed individuals is obtained from published data and is taken as $I_d(0) = 6$. We assume the initial number of recovered individuals is zero, i.e., R(0) = 0.

Parameter values. The average life expectancy of the people in Dougherty county is 75.05 years.³⁸ Thus, the natural death rate is $\mu = \frac{1}{75.05 \times 365}$ per day. Assuming the steady-state level before the start of the epidemics, we set $\Lambda - \mu S_0 = 0$, where S_0 is the total population before the start of the epidemic. Thus, the recruitment rate is $\Lambda = \frac{1}{75 \times 365} S_0$ per day. Since the average incubation period of COVID-19 is 5.2 days,¹⁷ we take $\eta = \frac{1}{5.2}$ per day. The infected individuals either die or recover. The total number of reported cases in Dougherty County between 21 March 2020 and 25 March 2021, is 6815, among which 283 died.³⁴ Thus, the probability that a diagnosed patient dies can be approximated as 0.042. Also, an infected individual leaves the compartment in about 17 days on average.¹⁷ Assuming the same death rate for both diagnosed and undiagnosed individuals, we obtain $\delta_u = \delta_d = 0.042 \times \frac{1}{17} = 0.0025$, which implies the recovery rate to be $\lambda = (1 - 0.042) \times \frac{1}{17} = 0.056$ per

day. Note that taking a reduced value for the death rate of undiagnosed infected individuals does not make any significant difference in our conclusions.

Vaccination strategy. Based on the currently implemented two-dose vaccines by Pfizer and Moderna, we take 25 days apart (Pfizer 21 days, Moderna 28 days) between the first and the second doses of the vaccines.³⁰ For the base case, we assume that 60% of the susceptible people get the first dose of vaccine within 5 months, and 85% of the vaccinated people with the first dose will get the second dose within 25 days of their first dose plus an additional 14 days for the vaccines to be fully effective. Then solving $\frac{dS}{dt} = -\nu_1 S$, we get $\nu_1 = -\frac{\ln(S(t)/S_0)}{t}$. With this formulation, if 60% population are vaccinated within 5 months (150 days), we require $\nu_1 = 0.006$. Also, for the individuals who have got first dose of the vaccine, we assume 85% of them get second dose and become highly protected in the next within 39 days such that $\nu_2 = \frac{0.85}{39} = 0.022$. The Pfizer mRNA vaccine shows efficacy, ranging from 52.4% to 68.5%, with the first dose only and 92% after completing the second dose.³⁹ Therefore, we assume that the first dose of the vaccine provides about 65% protection, implying $\alpha_1 = 0.35$, and the both doses of the vaccination provide 92% of the protection, implying $\alpha_2 = 0.08.$

Data fitting procedure. The transmission rate (β) , diagnosis rate (γ) , the initial value of Exposed class (E(0)), and the initial value of Undiagnosed Infected class $(I_u(0))$ are estimated by fitting the model to daily reported cases (smoothed by averaging weekly) in Dougherty County.³⁴ Since the number of reported cases show a time-varying trend depending on the timing of intervention policies and public events, we assume that two parameters, $\beta = \beta(t)$ and $\gamma = \gamma(t)$, are time-dependent. We then use the optimization techniques to estimate these two parameters for each of the intervals associated with the timing of intervention policies and public events. Specifically, we use the local optimization solver fmincon in MATLAB to find the local minimum and the global optimization toolbox multistart, which uses several uniformly distributed starting points. Thus, in our data fitting process, the local solver fmincon first finds local optima representing the best fit of the model to the data, and then the process is repeated multiple times via the multistart algorithm, allowing a more thorough search for a global minimum.⁴⁰

3.3. Model versus data

All the parameters and initial values of the state variables are provided in Table 1, and the estimated values of β and γ for each interval are provided in Table 2.

The weekly averaged data of reported cases in Dougherty County and the model estimates for the diagnosed cases together with the major events in Dougherty county are presented in Fig. 2. Our model fits the data well (Fig. 2), thereby validating our model for the COVID-19 transmission dynamics in Dougherty county.

Variable	Units	Initial Value	References
\overline{S}	people	86,712	36, 37
V_1	people	0	41
V_2	people	0	41
E	people	1	Fitted
I_u	people	55	Fitted
I_d	people	6	34
R	people	0	Assumed
Parameter	Units	Value	References
Λ	people $* day^{-1}$	3.16	38, 36, 37
μ	day^{-1}	$\frac{1}{75.05 \times 365}$	38
α_1	NA	0.35	Assumed
α_2	NA	0.08	Assumed
ν_1	day^{-1}	0.006	Assumed
ν_2	day^{-1}	0.022	Assumed
η	day^{-1}	0.19	17
$\stackrel{'}{\lambda}$	day^{-1}	0.056	17
δ_u	day^{-1}	0.0025	Calculated
δ_d	day^{-1}	0.0025	Calculated

Table 1. The initial values of state variables and parameter values of model (2.1).

Table 2. Estimated values of the transmission rate (β) and the diagnosis rate (γ) for each interval.

Intervals	β	γ
3/21/2020-4/10/2020	1.14×10^{-5}	0.85
4/10-6/21	1.63×10^{-6}	0.89
6/21-7/11	8.87×10^{-6}	0.61
7/11-11/17	3.39×10^{-6}	0.86
11/17-12/14	6.22×10^{-6}	0.28
12/14-12/28	1.36×10^{-6}	0.33
12/28/2020-1/11/2021	3.33×10^{-6}	0.23
1/11-3/25	6.21×10^{-7}	0.32

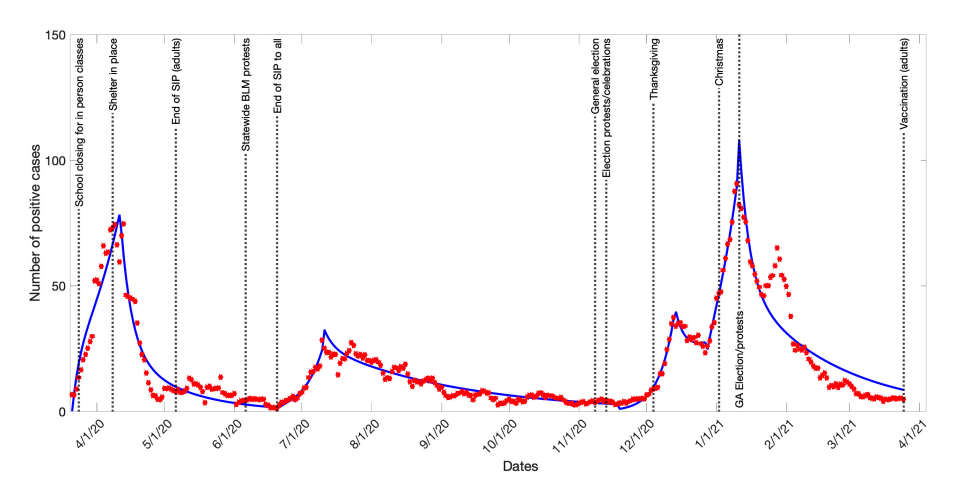


Fig. 2. The COVID-19 Pandemic data (weekly average in red dots) of number of daily positive cases and the model estimation (blue curve) in Dougherty County, GA.

4. Characteristic of Epidemic in Dougherty County

4.1. Transmission patterns

From Fig. 2, we observe that the initial surge of the COVID-19 reported cases started to decline shortly after the implementation of intervention policies such as school closure (started on 18 March 2020), social distancing with restriction on the public gathering (started on 23 March 2020), and shelter-in-place (on 2 April 2020). The shelter-in-place for adults ended on 30 April 2020, but was still active for seniors and immune-compromised people until 14 June 2020. The state-wide protests and end of the shelter-in-place triggered the second surge of the cases in late June and early July of 2020. The activities and gatherings related to the general election, gatherings during festivals such as Thanksgiving and Christmas triggered multiple surges with the all-time high number of cases towards the end of 2020. Our estimates show that the transmission rates are high during three interval periods (Table 2), at the beginning of March 2020, in the middle of June 2020, and towards the end of 2020 (after November 17).

The dynamics of undiagnosed people and the total number of infectious people in the county are presented in Fig. 3. We observe that the number of undiagnosed

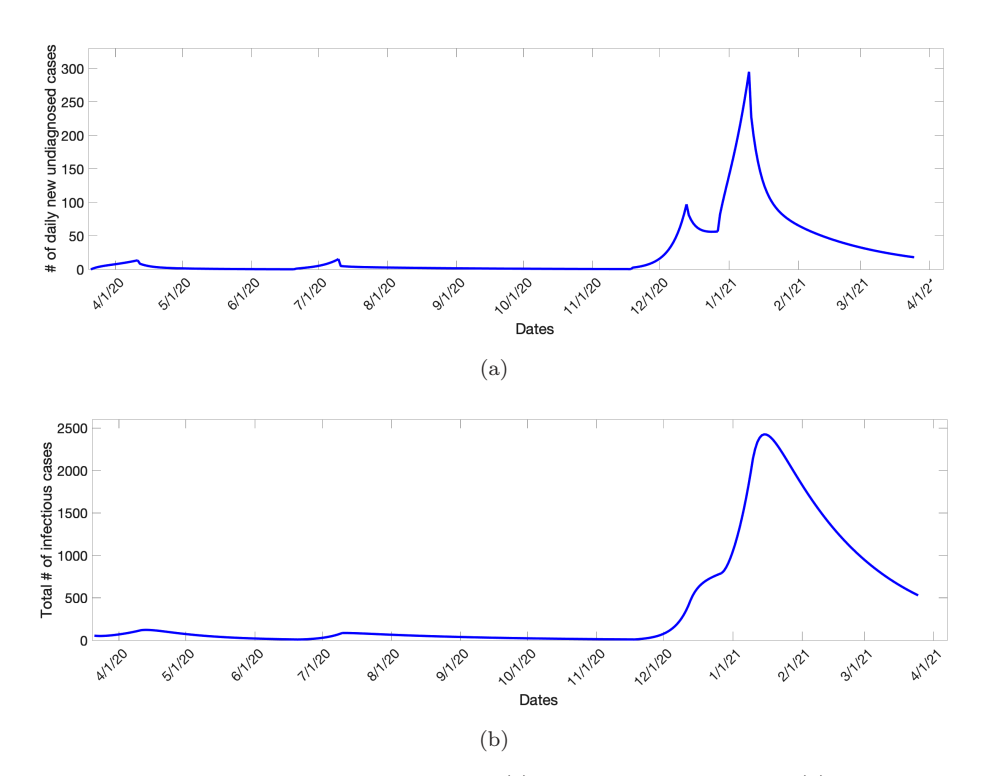


Fig. 3. The number of daily undiagnosed cases (a) and total infectious cases (b) under no vaccination strategy $\nu_1=\nu_2=0$.

people and the number of infectious people follow similar trends as reported cases. The highest peak of undiagnosed and infectious individuals are estimated to be 295 and 2425, respectively, at around 10 January 2021, right after the GA election with sharp increase beginning from the general election day (3 November 2020). These numbers are about 25 folds higher than the peaks in earlier waves on 13 April 2020, and 11 July 2020. These results imply that events that caused public gatherings, such as elections, protests, and festivals, contributed to the increase in infections. After mid-January of 2021, the number of new undiagnosed cases and the total number of infectious cases declined sharply. The phase-wise vaccinations started in mid-February helped to decrease these numbers further.

4.2. Basic reproduction number

In Sec. 2.2, we formulated the expression for the vaccination reproduction number, \mathcal{R}_{vac} . When $\nu_1 = 0, \nu_2 = 0$, the vaccination reproduction number \mathcal{R}_{vac} reduces to the basic reproduction number \mathcal{R}_0 , which is defined as the average number of secondary infections produced by a typical case of an infection in a population where everyone is susceptible. Taking the average values of the transmission rate (β) and diagnosis rates (γ) (weighted averages from Table 2) and other parameters from Table 1, the value of the basic reproduction number is $\mathcal{R}_0 = 1.69$. We also compute the basic reproduction number, \mathcal{R}_0 , for various values of the transmission rate (β) and the diagnosis rate (γ) with all other parameters fixed at their base value given in Table 1 (Fig. 4). We observe that a higher diagnosis rate or a lower transmission rate provides a lower value of \mathcal{R}_0 as expected. For example, for a 10% diagnosis rate and a transmission rate of $\beta = 4.655 \times 10^{-6}$, we get \mathcal{R}_0 to be 6.18, indicating the occurrence of an outbreak, while an increase of the diagnosis rate to 90% with the same transmission rate brings \mathcal{R}_0 to 0.71, indicating the disease is under control. We found that the value of \mathcal{R}_0 is less than 1 for any value of γ if the value of β is less than 6.897×10^{-7} . This highlights the importance of intervention policies that reduce the contacts between individuals bringing β below 6.897×10^{-7} to control the disease spread.

4.3. Effective reproduction number

The basic reproduction number is calculated with the assumption that the individuals in an entire community are susceptible to COVID-19. This assumption is valid at the beginning of the epidemic since there are only a few infected individuals and intervention measure such as vaccination is not implemented. However, as time progresses, infected individuals may get immunity by infection or vaccinations and are no longer susceptible to the disease. Also, intervention policies can make individuals less susceptible. Thus, a single value representing the average number of secondary infections throughout the whole outbreak may not provide the

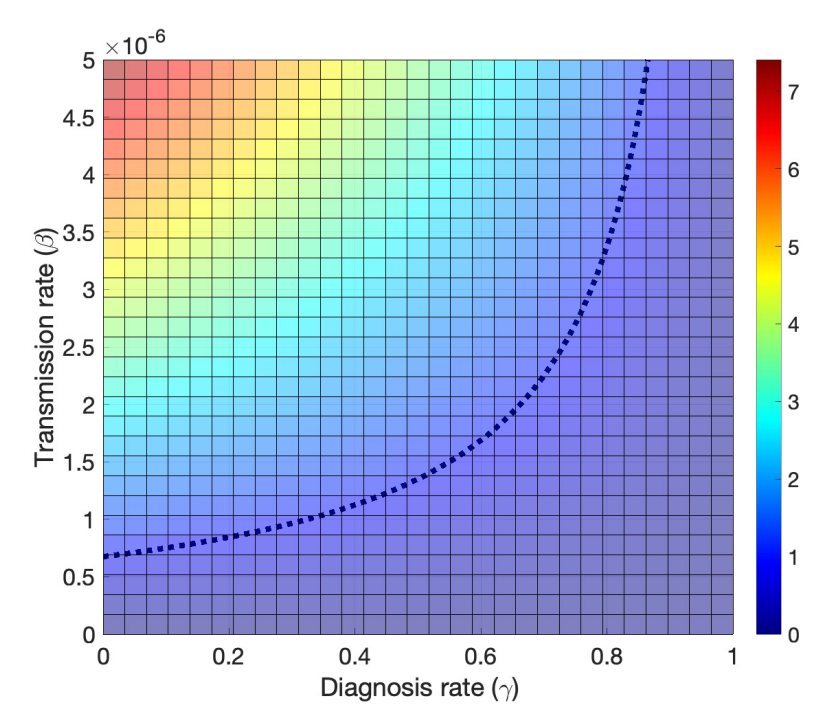


Fig. 4. \mathcal{R}_0 for various values of diagnosis rate (γ) and transmission rate (β) . The dotted line corresponds to $\mathcal{R}_0 = 1$.

complete picture of the epidemic trend. For the time-dependent change, we evaluate the effective reproduction number, \mathcal{R}_t . The value of \mathcal{R}_t indicates whether the outbreak is expanding $(\mathcal{R}_t > 1)$ or diminishing $(\mathcal{R}_t < 1)$ at each time point t. For our model, the expression for the time varying reproduction number is given by

$$\mathcal{R}_t = \frac{\beta(t)\eta(1-\gamma(t))(\alpha_1 V_1(t) + \alpha_2 V_2(t) + S(t))}{(\eta+\mu)(\lambda+\mu+\delta_u)}.$$

As shown in Fig. 5, the value of \mathcal{R}_t ranges from 0.26 to 6.36. The higher values of \mathcal{R}_t are observed after the end of restriction policies, such as the end of shelter-in-place, and after major public events that trigger mass gatherings, such as festivals and elections, and \mathcal{R}_t usually starts to decrease after about two weeks of those events. The highest value of \mathcal{R}_t is observed after the general election on 3 November 2020, followed by during the major holidays. The lowest value of \mathcal{R}_t is observed after the implementation of shelter-in-place and restriction in gathering and social distancing. This shows that the non-pharmaceutical intervention policies, such as shelter-in-place, restriction in gathering, school closures, were effective in lowering the COVID-19 transmission in Dougherty county.

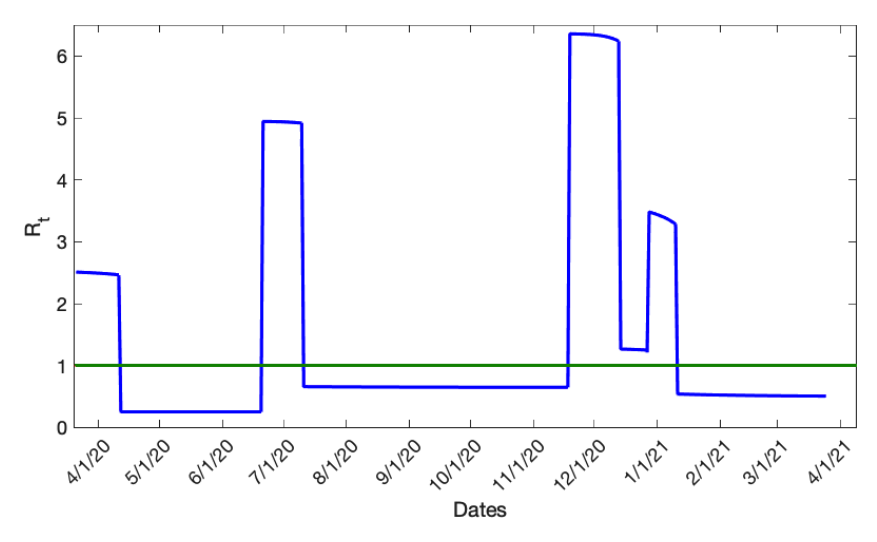


Fig. 5. The effective reproduction number \mathcal{R}_t at different intervals. The horizontal green line represents the threshold value for the disease spread. That is, $\mathcal{R}_t = 1$.

5. Role of COVID-19 Vaccination

In this section, we present the impact of vaccination programs on disease dynamics. Note that the number of reported cases in mid-March of 2020 is similar to the time after one year when the vaccination program was initiated in Dougherty county. Therefore, we expect that the implementation of vaccination programs on the previous year results in similar outcomes, at least qualitatively, to the year 2021. Hence for the purpose of demonstration, we present the results with vaccination programs implemented for the periods for which the data are considered (21 March 2020 to 25 March 2021).

5.1. Effects on reproduction numbers

As discussed in Sec. 3.2, people vaccinated with one dose and both doses may be infected with the virus but with different rates. Here, we evaluate the effect of various vaccination rates and transmission rates on the value of vaccination reproduction number \mathcal{R}_{vac} . In Fig. 6, we present the values of \mathcal{R}_{vac} for various vaccinations and transmission rates with all other parameters fixed at their base values.

Our model shows that if the first dose vaccination rate (ν_1) is above 0.0011, \mathcal{R}_{vac} remains less than 1 (i.e., the disease does not spread) for any rate of the second dose vaccination, ν_2 (Fig. 6(a)). The vaccination rate for the second dose has a lesser impact on the value of \mathcal{R}_{vac} . For example, with the first dose vaccination rate at its minimum value, $\nu_1 = 10^{-5}$, the value of \mathcal{R}_{vac} changes from 1.43 to 1.35 on increasing value of ν_2 from 10^{-5} to 5.7 × 10^{-2} . On the other hand, with the fixed

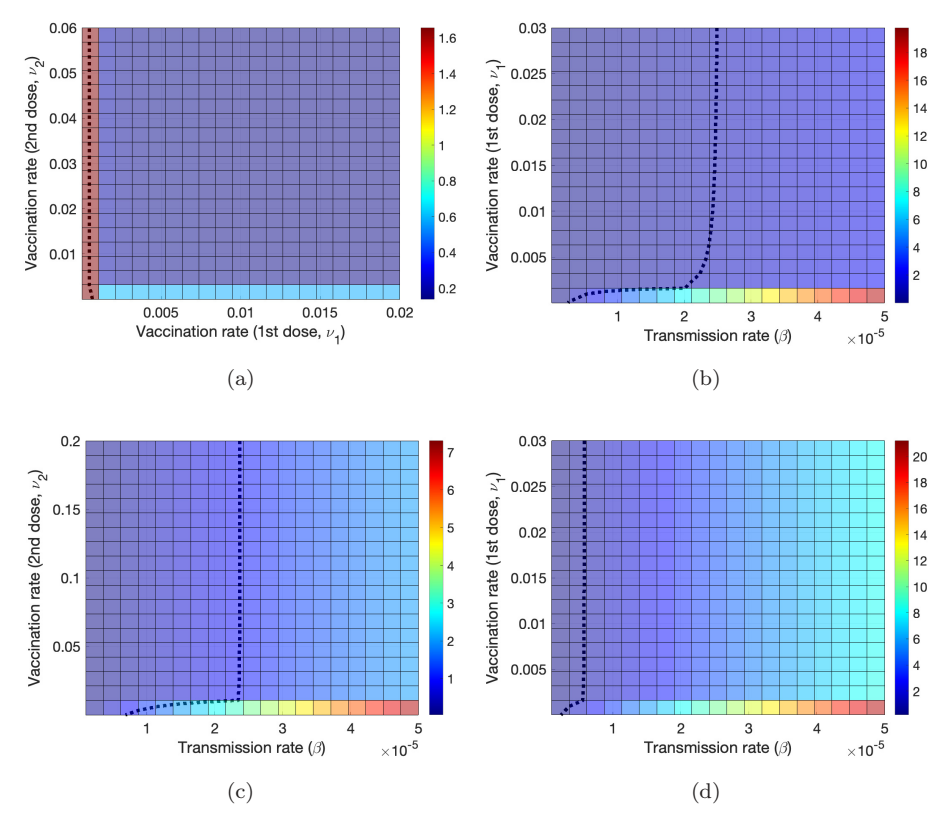


Fig. 6. The values of \mathcal{R}_{vac} for various combinations of (a) Vaccination rates ν_1 and ν_2 , (b) Transmission rate (β) and first dose vaccination rate (ν_1), (c) Transmission rate (β) and second dose vaccination rate (ν_2), and (d) Transmission rate (β) and first dose vaccination rate (ν_1) in the absence of the second dose ($\nu_2 = 0$).

second dose vaccination rate at its minimum value $\nu_2 = 10^{-5}$, an increase of the first dose vaccination rate from 10^{-5} to 1.9×10^{-2} can reduce the value of \mathcal{R}_{vac} from 1.43 to 0.49, where the average values of transmission and diagnosis rates $(\beta = 3.4221 \times 10^{-6} \text{ and } \gamma = 0.6673)$ are used in the calculation that are weighted over the length of the interval given in Table 2. As shown in Fig. 6(b), we observe that for smaller transmission rates $(\beta < 2.37 \times 10^{-5})$, the first dose vaccination rate (ν_1) is greater than 0.002 can bring the value of \mathcal{R}_{vac} below unity. Nevertheless when the transmission rate exceeds 2.64×10^{-5} , \mathcal{R}_{vac} remains larger than unity regardless of the value of ν_1 , implying that the vaccination program alone may not be sufficient to control the disease if the transmission rate is high. Therefore, at a high-transmission scenario, the vaccination programs should be accompanied by other non-pharmaceutical strategies that restrict contacts between people lowering the transmission rate.

For a fixed first dose vaccination rate at $\nu_1 = 0.015$, our model simulations (Fig. 6(c)) show that if the rate of vaccination of second dose, ν_2 , is greater than

0.001, the value of \mathcal{R}_{vac} can be brought to below unity by making the transmission rate, β , less than 2.68×10^{-5} . However, if the transmission rate, β is greater than 2.68×10^{-5} , the value of \mathcal{R}_{vac} exceeds unity regardless of the value of ν_2 . In Fig. 6(d), we present \mathcal{R}_{vac} for various transmission rates and the first dose vaccination rate when the second dose vaccination is absent (i.e., $\nu_2 = 0$). In this case, the value of \mathcal{R}_{vac} exceeds unity for all rates of the first dose vaccination considered if the transmission rate is higher than 6.16×10^{-6} . These results imply that if the transmission rates are low (for example, $\beta < 6.16 \times 10^{-6}$), then dropout from the second dose vaccine may not have a significant impact on the disease spread, but in case of a higher transmission rate, the spread may become uncontrollable ($\mathcal{R}_{\text{vac}} > 1$) if the second dose of the vaccines is dropped.

Next, we present the effective reproduction number for various vaccination scenarios. In Fig. 7, we present the plots for \mathcal{R}_t under three vaccination scenarios: no vaccination ($\nu_1 = 0, \nu_2 = 0$, no vaccination), vaccination with single dose only ($\nu_1 = 0.006, \nu_2 = 0$, incomplete vaccination) and vaccination with both doses ($\nu_1 = 0.006, \nu_2 = 0.022$, complete vaccination). We observe that the vaccination reduces the value of effective reproduction number. For example, under no vaccination and under incomplete vaccination, the effective reproduction number, \mathcal{R}_t , exceeds 1 in three time intervals while it exceeds 1 in only two time intervals if the vaccination is completed. Thus, there is an additional time interval where the disease spread if vaccination is not provided or incomplete. Also the magnitude of

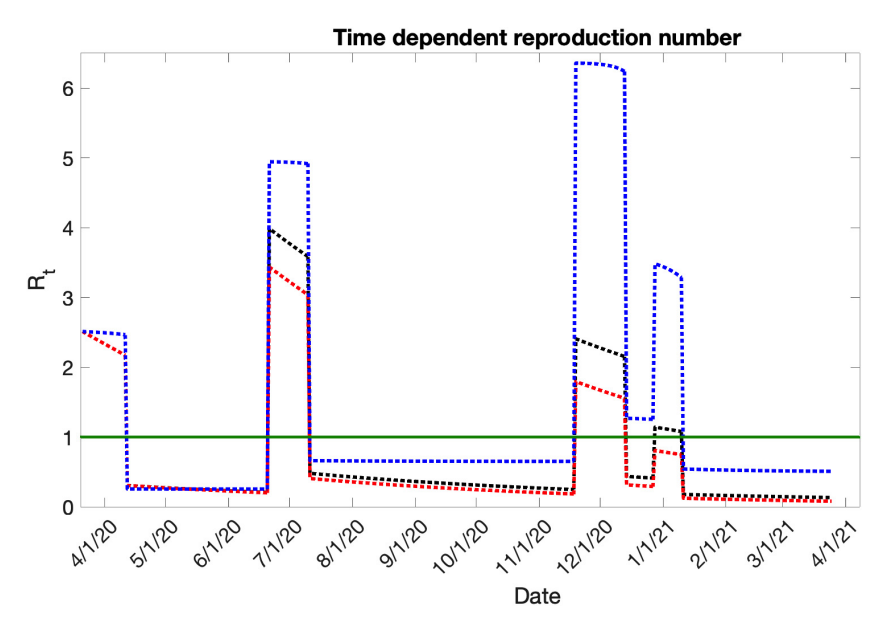


Fig. 7. The time-dependent reproduction number \mathcal{R}_t without vaccination (blue curve), with one dose (incomplete) vaccination (black curve) and both dose (complete) vaccination (red curve). The horizontal green line indicates the threshold value for the disease spread, i.e., $\mathcal{R}_t = 1$.

the \mathcal{R}_t gets as high as 6 (11/15/2020–12/15/2020) if no vaccine is administered, while the maximum value is, respectively, 2.5 and 2 under incomplete and complete vaccination. This shows the magnitude of \mathcal{R}_t is reduced significantly if at least one dose of vaccine is administered.

5.2. Effects on cases and incidence

In this section, we study the effect of vaccination in number of daily undiagnosed cases and total number of infectious cases. We consider a slower and a faster vaccination strategies. Under the slower vaccination, we assume 60% of the people get the first dose within a year and similarly under the faster vaccination, we assume that 60% of the people get first dose within two months. In both cases, we assume that 85% of the people who get the first dose get the second dose 25 days and an additional 14 days for full immunity induced by the vaccine. Thus, for slower strategy, the vaccination rates should be $\nu_1 = 0.0025$ and $\nu_2 = 0.022$ and for the faster strategy, the rates are $\nu_1 = 0.015$ and $\nu_2 = 0.022$. Our model predictions for daily undiagnosed cases and the infectious cases under the three (base, slower and faster) vaccinations with complete (both doses) and incomplete (a single dose) vaccinations are presented in Fig. 8.

From the figure, we observe that under both complete or incomplete vaccinations, the number of daily undiagnosed cases and total infectious cases show similar trend at the initial phase of the outbreak regardless of the vaccination paces. But these numbers are significantly higher in the later phase if the vaccination is slower (Figs. 8(a) and 8(c)). For example, in the base case under complete vaccination, the number of daily undiagnosed cases and the total number of infectious cases decline to \sim zero around September 2020 (red curve Figs. 8(a) and 8(c)), while

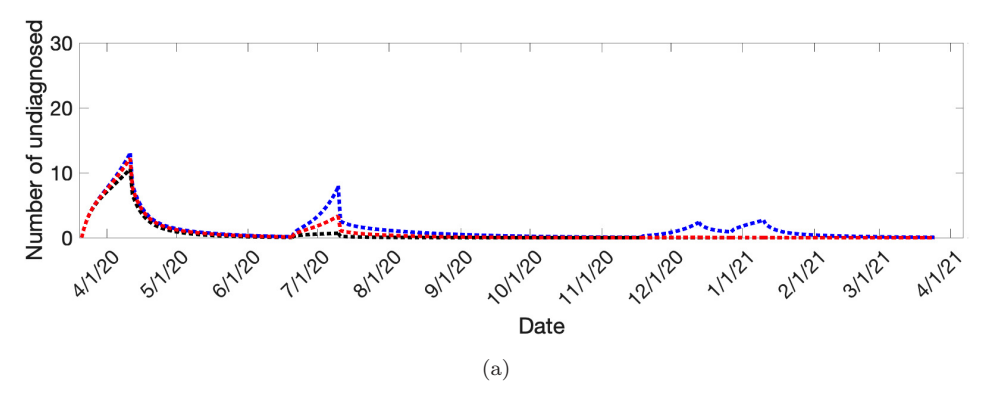


Fig. 8. The number of daily undiagnosed cases under complete vaccinations (a) and incomplete vaccination (b) and infectious cases under complete vaccinations (c) and incomplete vaccination (d) under slow (blue dotted curve), fast (black dotted curve) and base (red dotted curve) vaccination strategies.

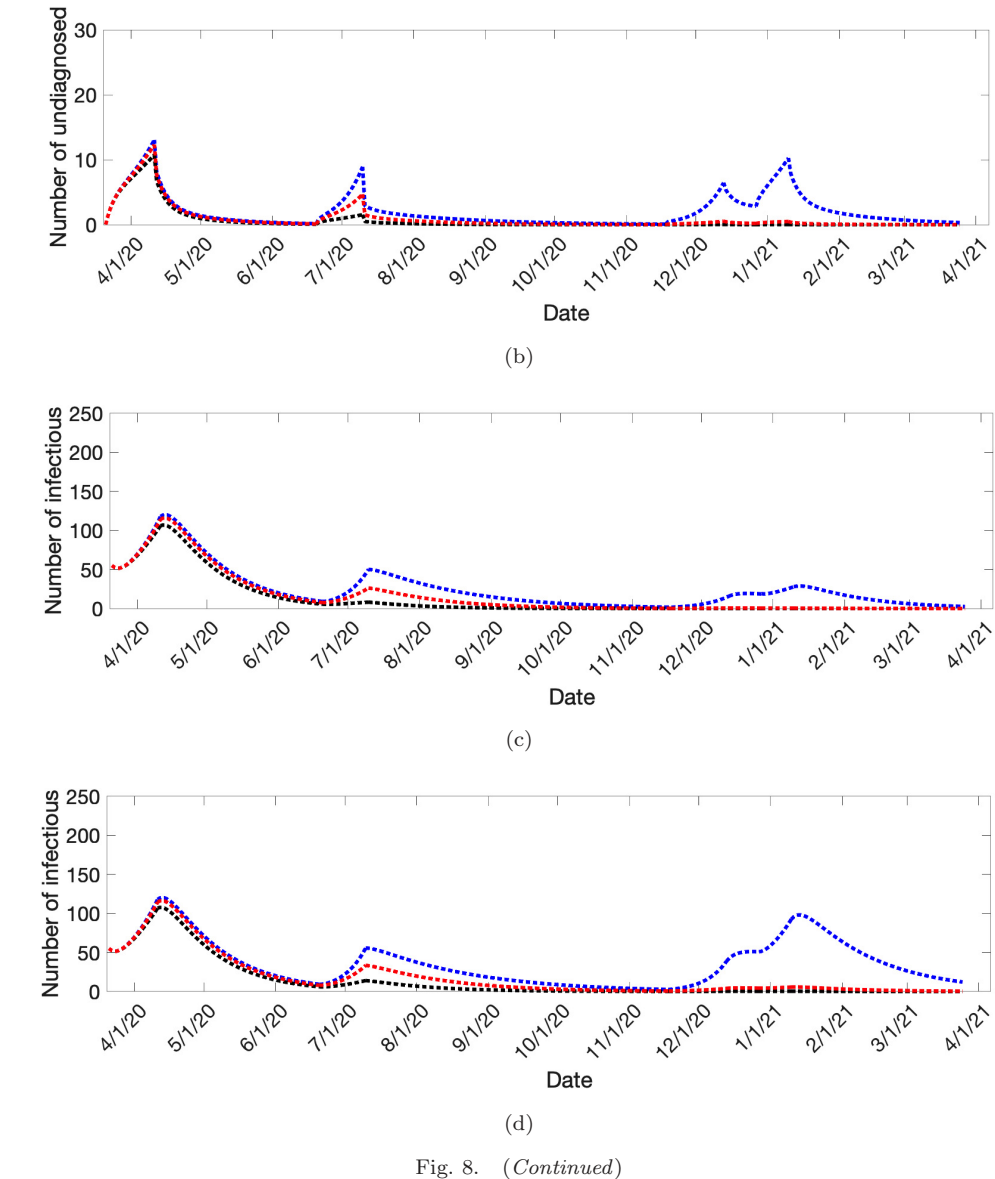


Fig. 8.

it takes until November 2020 under the slow vaccination strategy and these numbers increase again after the mid November and stay positive until March 2021 (Figs. 8(a) and 8(c)). Similarly, under complete vaccination with faster pace, these numbers decline to zero faster, around August 2020 (see Figs. 8(a) and 8(c)). Similarly, under the incomplete vaccination, both daily undiagnosed cases and total infectious cases are similar until the last week of June 2020 regardless of the pace of vaccination (Figs. 8(b) and 8(d)). But these numbers increase significantly in later phase compared to the complete vaccination. For example, in 8 January 2021, the total number of daily undiagnosed and infectious cases were, respectively, 3 and 29 under complete vaccinations and slower pace while these numbers are 11 and 98 under incomplete vaccination which is about 300% increase on that date. This implies that completion of the both doses of vaccine is crucial to lower the disease burden.

In Fig. 9, we present the above simulations to see how a slight delay in the start of the vaccination program impacts the transmission trend. Assuming a two months delay in the start of the vaccination, we observe that the daily undiagnosed cases and the total number of infectious cases increase significantly in the later phase under both complete and incomplete vaccination strategies compared to no delay. For example, under complete vaccination with slower pace and without delay, the daily undiagnosed cases and total infectious cases around the first week of July 2020 peaked to about 9 and 49 cases, respectively (Figs. 8(a) and 8(c)) while

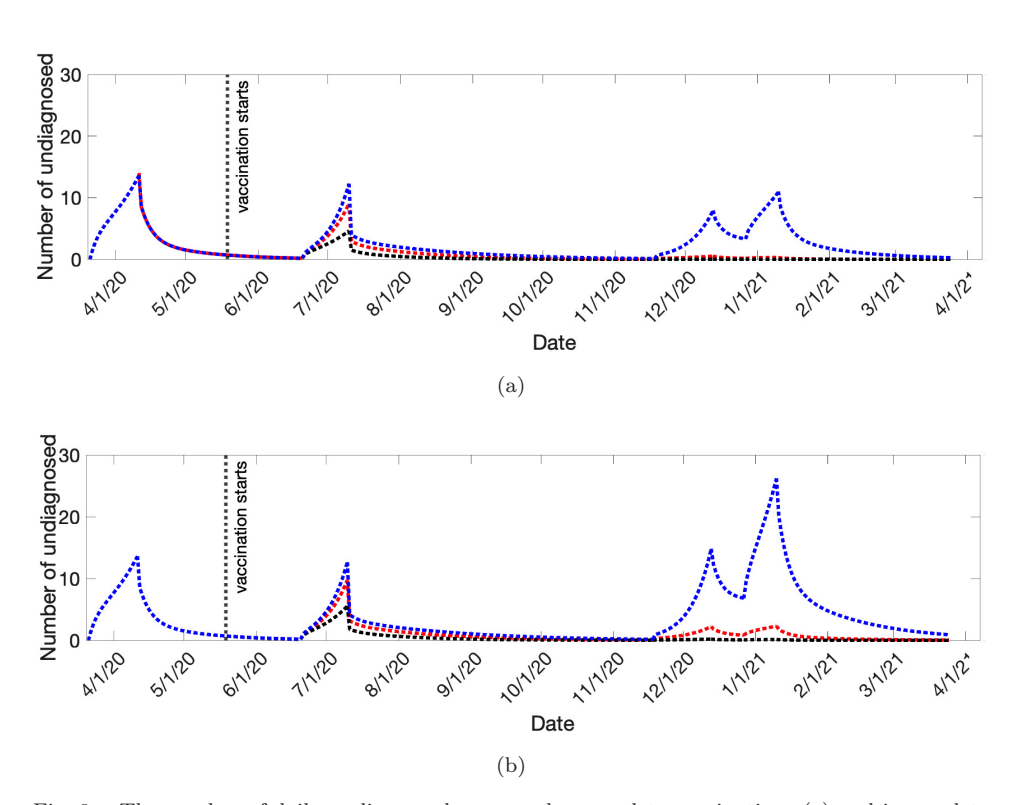
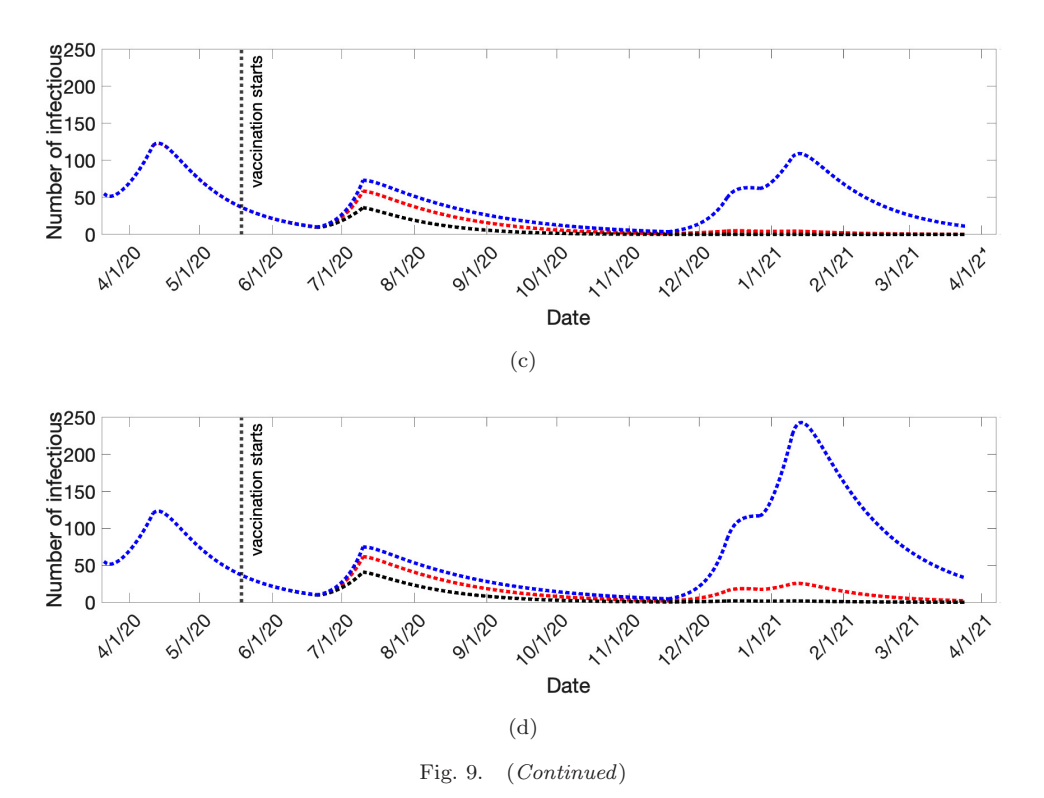


Fig. 9. The number of daily undiagnosed cases under complete vaccinations (a) and incomplete vaccination (b) and infectious cases under complete vaccinations (c) and incomplete vaccination (d) under slow (blue dotted curve), fast (black dotted curve) and base (red dotted curve) vaccination strategies when the vaccination is started after two months delay of the first diagnosed case.



these numbers are 13 and 73 with two months delay (Figs. 9(a) and 9(c)) causing about 44% and 62% increases, respectively, caused by the delay. Under the fast vaccination strategy, we do not observe much difference in the trends with and without delay in the start of vaccination. Similarly, under incomplete vaccination with delay, the number of daily undiagnosed cases and number of infectious cases are much higher compared to other complete and without delay strategies (Figs. 9(b) and 9(d)). For example, under slow and incomplete vaccination without delay, the number of daily undiagnosed and total infectious cases on 8 January 2021 are 10 and 98, respectively (Figs. 8(b) and 8(d)), while these numbers are 26 and 240 if the vaccination is delayed (Figs. 9(b) and 9(d)). Hence, we conclude that impact of delay is more under slower vaccination strategy. Also, in the long run, the faster vaccination strategy is much better than other vaccination pace in both with or without delay.

We now evaluate the incidence during the entire study period for various vaccination rates and transmission rates with all other parameters fixed at their base values (Tables 1 and 2). From our model, the total incidence is given by the following integral:

$$\label{eq:Incidence} \text{Incidence} = \int_0^{t_f} (\beta S I_u + \beta \alpha_1 I_u V_1 + \beta \alpha_2 I_u V_2) dt.$$

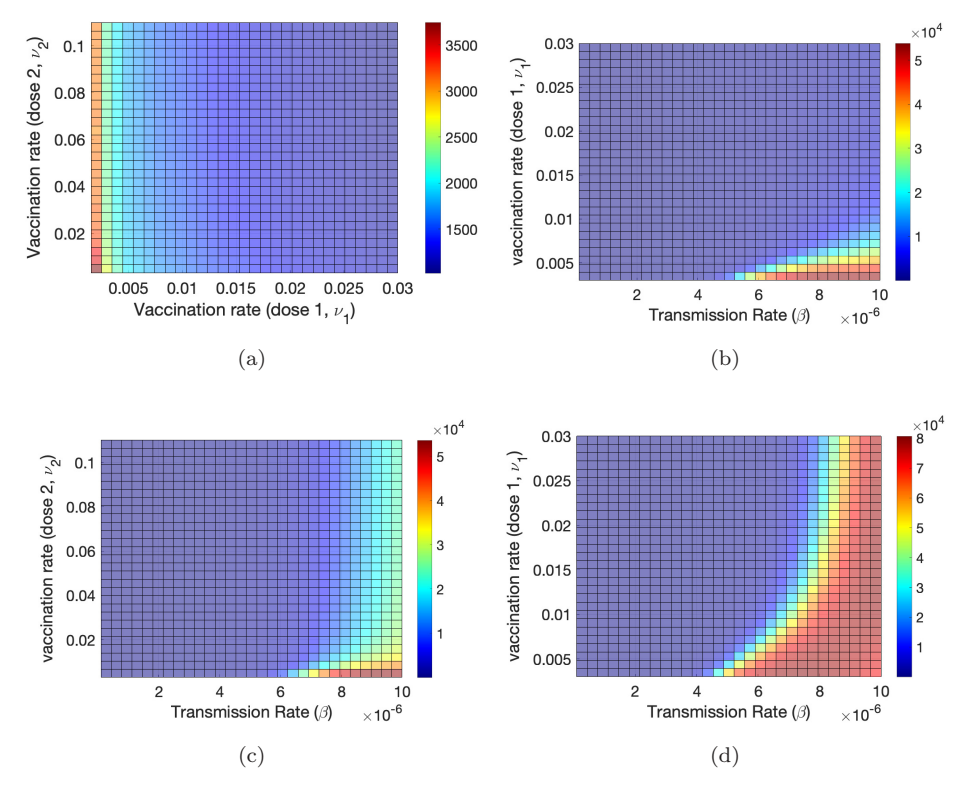


Fig. 10. The total incidence for various combinations of (a) Vaccination rates (ν_1 and ν_2) (b) Transmission rate (β) and vaccination rate (first dose, ν_1), (c) Transmission rate (β) and vaccination rate (second dose, ν_2) and (d) Transmission rate (β) and vaccination rate (first dose, ν_1), when $\nu_2 = 0$.

Here, t = 0 represents the beginning of our study period, i.e., 21 March 2020, while $t = t_f$ represents the total time for the entire study period, i.e., from 21 March 2020 to 25 March 2021.

As shown by our simulation results (Fig. 10(a)), the first dose vaccination rate is more impactful in reducing the total incidence compared to the second dose. For example, when the first dose vaccination rate is $\nu_1 = 0.0015$ and the second dose vaccination rate is $\nu_2 = 0.003$, the total incidence is 3746, which reduces to 1162 (about 69% reduction) if the first dose vaccination rate is increased to 0.03 keeping the same rate for second dose vaccination. On the other hand, if the second dose vaccination rate is increased to $\nu_2 = 0.06$, the total incidence reduces to only 3023 (only 20% reduction).

In Figs. 10(b) and 10(c), we show that the total incidence increases as the transmission rate increases, but with a higher vaccination rate (both first and second doses), the total incidence does not grow significantly even with a higher transmission rate. For example, if the vaccination rate is small ($\nu_1 = 0.003$, $\nu_2 = 0.022$), the total incidence for a small transmission rate ($\beta = 10^{-7}$) is 7 while the total

incidence for a bigger transmission rate ($\beta=10^{-5}$) is 53,800. But for a higher first dose vaccination rate ($\nu_1=0.03,\,\nu_2=0.022$), the total incidence for the small transmission rate ($\beta=10^{-7}$) and the bigger transmission rate ($\beta=10^{-5}$) are 5 and 2,231, respectively. Similarly, when the second dose vaccination rate is low ($\nu_2=0.003,\,\nu_1=0.015$), the total incidence for a small transmission rate ($\beta=10^{-5}$) is 6 while the incidence for a bigger transmission rate ($\beta=10^{-5}$) is 22,290. Nevertheless, when the second dose vaccination rate is high ($\nu_2=0.06$), the total incidence for the low transmission rate ($\beta=10^{-7}$) is 6, while the incidence for the higher transmission rate ($\beta=10^{-5}$) is 4151. Hence, the vaccination is much more impactful when the transmission rates are higher.

In Fig. 10(d), we present the model predicted total incidence for various transmission rates and the first dose vaccination rate in the absence of second dose vaccination ($\nu_2 = 0$). In this case, more people are infected as expected. For example, with a small transmission rate ($\beta = 10^{-7}$), the total incidence with a small first dose vaccination rate is 7, but when the transmission rate increases to 9×10^{-6} , the total incidence increases to 75,400. Similarly, when the first dose vaccination rate is higher ($\nu_1 = 0.03$), the total incidence for the higher transmission rate ($\beta = 9 \times 10^{-6}$) is 63,470. Since the total incidence for the higher transmission rate remains significantly high even with a higher first dose vaccine if the second dose vaccine is not administered. Therefore, taking both doses of the vaccines is crucial in controlling the disease via vaccination programs.

6. Conclusion

COVID-19 is a massive problem in many places, devastating almost every aspect of human life by infecting and killing millions of people. Although the development of effective vaccines helped to subside new cases to some extent, the emergence of new virus strains posed a risk in many parts of the world. Also, the limited availability of vaccines, public hesitation to vaccinations, and inability to complete the second dose of vaccine are some other obstacles to fully return to pre-pandemic normal state.⁵

In this work, we developed a novel mathematical model including two vaccinated compartments: vaccinated with the first dose and both doses. We thoroughly analyzed our model for the existence, stability and persistence of the solutions and derived expressions for reproduction numbers. We compiled the daily reported COVID-19 case data of Dougherty County of Georgia, USA, and used the data to estimate model parameters. We observed that the surge in the COVID-19 cases occurred after the lifting of the restriction policies, after increasing human activities such as protests and gatherings, and public holidays. The cases declined after the implementation of restrictions in public gatherings, social distancing, shelter-in-places, and the start of vaccination.

Our model estimates that during the peak of the pandemic, the effective reproduction number in the county reached as high as 6.36, and the number of undiagnosed cases reached about three times higher (295 per day) than the maximum number of reported cases (90 in a day). Our study emphasizes the need for the completion of both doses of vaccine (if it requires two doses) to control the disease in the low transmission scenario, but in case of the high transmission, only vaccinations may not be enough to contain the disease. Thus, in the high-transmission case, other intervention strategies that reduce the transmission rate may be required. Also, a faster vaccination strategy is the best even if there is some delay compared to the other vaccination strategies considered.

We acknowledge some limitations in our study. We considered transmission from undiagnosed infected individuals only assuming that all diagnosed individuals are isolated and do not transmit the disease. This may not always be the case. We did not include the movement of people in and out of the county as surges in other counties in the state of Georgia may have partially contributed to the surge in Dougherty county. Inclusion of emigration or immigration in the model and the corresponding data may better predict the outbreak. We considered the constant vaccination rate throughout the outbreak. The extension of our model with time-dependent vaccination rates and formulation of optimal policies would be useful. Also, we did not consider the potential waning of vaccine immunity as the quantitative understanding of the loss of vaccine immunity is limited. Incorporating the accurate decline of vaccination immunity could provide better insight into the trend of the outbreak in the long run.

Acknowledgments

The work of NKV was partially supported by NSF grants DMS-1951793, DMS-1836647, and DEB-2030479 from the National Science Foundation of USA, and the UGP award from San Diego State University. The work of JMA was partially supported by NSF grants DMS-2052355.

References

- CDC, COVID-19, Centers for Disease Control and Prevention, Atlanta, GA, 2021, https://www.cdc.gov/coronavirus/2019-ncov/.
- 2. Worldmeter, Coronavirus, 2020, Worldmeter, United States of America, https://www.worldometers.info/coronavirus/.
- 3. IHME-COVID-19-Forecasting-Team, Modeling COVID-19 scenarios for the United States, Nat Med 27:94–105, 2021, https://doi.org/10.1038/s41591-020-1132-9.
- CNN, With the more contagious Delta variant, some officials are issuing new
 mask guidance, 2021, Cable News Network, New York, https://www.cnn.com/2021/
 06/29/health/ us-coronavirus-tuesday/index.html.
- Abc News, 2nd vaccine shot statistics show majority getting it, only 5 million missing CDC, New York, 2021, https://abcnews.go.com/Health/millions-missing-2nd-vaccine-dose-rounds-cdc/story?id=77300383.
- NYTimes, Days After a Funeral in a Georgia Town, coronavirus Hit Like a Bomb, 2020, New York Times, New York, https://www.nytimes.com/2020/03/30/us/ coronavirus-funeral-albany-georgia.html.

- 7. Business-Insider, How a small Georgia city far from New York became one of the worst coronavirus hotspots in the country, 2020, Business Insider, New York, https://www.businessinsider.com/coronavirus-hotspot-albany-georgia-funderals-covid-19-cases-per-capita-2020-4.
- 8. USNews, Southwest Georgia Hard-Hit as Virus Cases and Deaths Rise, 2020, US News, New York, https://www.usnews.com/news/best-states/georgia/articles/2020-03-20/coronavirus-cases-deaths-continue-to-rise-in-georgia.
- 9. CNN, How two funerals helped turn one small Georgia city into a hotspot for coronavirus, Cable News Network, New York, https://www.cnn.com/2020/04/02/us/albany-georgia-coronavirus/index.html.
- Kyrychko YN, Blyuss KB, Brovchenko I, Mathematical modelling of the dynamics and containment of COVID-19 in Ukraine, Sci Rep 10:10–19, 2020, https://doi.org/10.1038/s41598-020-76710-1.
- Ndaïrou F, Area I, Nieto JJ, Torres DFM Mathematical modeling of COVID-19 transmission dynamics with a case study of Wuhan, Chaos Solitons Fractals 135, 2020, https://doi.org/10.1016/j.chaos.2020.109846.
- Sun T, Wang Y, Modeling COVID-19 epidemic in Heilongjiang province, China, Chaos Solitons Fractals 138, 2020, https://doi.org/10.1016/j.chaos.2020. 109949.
- Alvarez MM, González-González E, Trujillo-de Santiago G, Modeling COVID-19 epidemics in an Excel spreadsheet to enable first-hand accurate predictions of the pandemic evolution in urban areas, Sci Rep 11, 2021, https://doi.org/10.1038/s41598-021-83697-w.
- Oliveira JF et al., Mathematical modeling of COVID-19 in 14.8 million individuals in Bahia, Brazil, Nat Commun 12(333), 2020, https://doi.org/10.1038/s41467-020-19798-3.
- Mugisha JYT, Ssebuliba J, Nakakawa JN, Kikawa CR, Ssematimba A, Mathematical modeling of COVID-19 transmission dynamics in Uganda: Implications of complacency and early easing of lockdown, PLoS One 16(2), 2020, https://doi.org/10.1371/journal.pone.0247456.
- 16. Tkachenko AV, Maslov S, Elbanna A, Wong GN, Weiner ZJ, Goldenfeld N, Time-dependent heterogeneity leads to transient suppression of the COVID-19 epidemic, not herd immunity, *Proc Natl Acad Sci* 118(17), 2021, https://doi.org/10.1073/pnas.2015972118.
- Adhikari K, Gautam R, Pokharel A, Uprety KN, Vaidya NK, Transmission dynamics of COVID-19 in Nepal: Mathematical model uncovering effective controls, *J Theor Biol* 521, 2021, https://doi.org/10.1016/j.jtbi.2021.110680.
- Pantha B, Acharya S, Joshi HR, Vaidya NK, Inter-provincial disparity of COVID-19 transmission and control in Nepal, Sci Rep 11, 2021, https://doi.org/10.1038/s41598-021-92253-5.
- 19. Moore S, Hill EM, Dyson L, Tildesley MJ, Keeling MJ, Modelling optimal vaccination strategy for SARS-CoV-2 in the UK, *PLOS Comput Biol* **17**(5), 2021, https://doi.org/10.1371/journal.pcbi.1008849.
- 20. Ferranna M, Cadarette D, Bloom DE, COVID-19 vaccine allocation: Modeling health outcomes and equity implications of alternative strategies, *Engineering* **7**(7):1–12, 2021, https://doi.org/10.1016/j.eng.2021.03.014.
- Bubar KM, Reinholt K, Kissler SM, Marc L, Cobey S, Yonatan HG, Larremore D, Model-informed COVID-19 vaccine prioritization strategies by age and serostatus, Science 371:916–921, 2021, https://doi.org/10.1126/science.abe6959.

- 22. Giordano G, Colaneri M, Filippo A, Blanchini F, Bolzern P, Nicolao G, Sacchi P, Colaneri P, Bruno R, Modeling vaccination rollouts, SARS-CoV-2 variants and the requirement for non-pharmaceutical interventions in Italy, *Nat Med* 27:993–998, 2021, https://doi.org/10.1038/s41591-021-01334-5.
- 23. Jentsch PC, Anand M, Bauch CT, Prioritising COVID-19 vaccination in changing social and epidemiological landscapes: a mathematical modelling study, *Lancet Infect Dis* **21**(8):1097–1106, 2021, https://doi.org/10.1016/S1473-3099(21)00057-8.
- 24. Mumtaz GR, El-Jardali F, Jabbour M, Harb A, Abu-Raddad LJ, Makhoul M, Modeling the impact of COVID-19 vaccination in Lebanon: A call to speed-up vaccine roll out, *Vaccines* 9(7):1–10, 2021, https://doi.org/10.3390/vaccines9070697.
- Moore S, Hill EM, Tildesley MJ, Dyson L, Keeling MJ, Vaccination and non-pharmaceutical interventions for COVID-19: A mathematical modelling study, *Lancet Infect Dis* 21(6):793–802, 2021, https://doi.org/10.1016/S1473-3099(21)00143-2.
- 26. Patel MD, Rosenstrom E, Ivy JS, Mayorga ME, Keskinocak P, Boyce RM, Lich KH, Smith III RL, Johnson KT, Delamater PL, Swann JL, Association of simulated COVID-19 vaccination and nonpharmaceutical interventions with infections, Hospitalizations, and Mortality, JAMA Netw Open 4(6), 2021, https://doi.org/10.1001/jamanetworkopen.2021.10782.
- 27. Childs L, Dick DW, Feng Z, Heffernan JM, Li J, Röst G, Modeling waning and boosting of COVID-19 in Canada with vaccination, medRxiv 2021, https://doi.org/10.1101/2021.05.18.21257426.
- 28. David WD, Childs L, Feng, Zhilan Z, Li J, Röst G., Buckeridge DL, Ogden NH, Heffernan JM, Fall 2021 Resurgence and COVID-19 Seroprevalence in Canada Modelling waning and boosting COVID-19 immunity in Canada A Canadian Immunization Research Network Study, medRxiv 2021, Cold Spring Harbor Laboratory Press, https://doi.org/10.1101/2021.08.17.21262188.
- Vignals C, Dick DW, Thiébaut R, Wittkop L, Prague M, Heffernan J, Barrier gesture relaxation during vaccination campaign in France: Modelling impact of waning immunity, 2021, https://doi.org/10.1101/2021.08.29.21262788.
- 30. CDC, COVID-19 Vaccinations, 2021, Centers for Disease Control and Prevention, Atlanta, GA, https://www.cdc.gov/vaccines/covid-19/index.html.
- Driessche PV, Watmough J, Reproduction numbers and sub-threshold endemic equilibria for compartmental models of disease transmission, Math Biosci 180:29–48, 2002.
- 32. Castillo-Chavez C, Feng Z, Huang W, Mathematical Approaches for Emerging and Reemerging Infectious Diseases: An Introduction, Springer-Verlag, Berlin, Germany, 2001
- 33. Thieme HR, Persistence under relaxed point-dissipativity (with application ton an endemic model), SIAM J Math Anal 24(2):7–435, 1993.
- 34. USAfacts, Dougherty County, Georgia coronavirus cases and deaths, 2021, USA facts, North America, https://usafacts.org/visualizations/coronavirus-covid-19-spread-map/state/georgia/county/dougherty-county.
- 35. News11, Medical professionals with coronavirus allowed to continue working after DPH 'mistake', 2020, News 11 Alive, Atlanta, https://www.11alive.com/article/news/health/coronavirus/dph-approves-message-medical-professionals-canwork-while-covid19-positive/85-3e682e89-3802-47c9-b3cf-5933f14834cb.
- 36. CBC, US Census, Dougherty County GA, 2019, United States Census Bureau, Suitland, MD, https://www.census.gov/quickfacts/doughertycountygeorgia.
- 37. WPReview, Dougherty County, Georgia Population 2020, 2020, World Population Review, United States, https://worldpopulationreview.com/us-counties/ga/dougherty-county-population.

- 38. Healthdata, County Profile: Dougherty County, Georgia, 2021, Healthdata.org, Seattle, Washington, http://www.healthdata.org/sites/default/files/files/county_profiles/US/2015/County_Report_Dougherty_County_Georgia.pdf.
- 39. Polack F et al., Safety and efficacy of the BNT162b2 mRNA COVID-19 vaccine, New Engl J Med 383:2603–2615, 2021, https://doi.org/10.1056/NEJMoa2034577.
- 40. Mathworks, Global optimization toolbox user's guide 2015a, 2015, *The Mathworks* Natic, MA.
- 41. Atlanta Journal Constitution, Trump supporters rally at Georgia Capitol, elsewhere in Atlanta, Atlanta Journal Constitution, 2021, Atlanta, GA, https://www.ajc.com/politics/election/trump-supporters-rally-at-georgia-capitol-elsewhere-in-atlanta/V4LEZAEPDJEAJ MNYX5UTDTLCNQ/.